

Evolutionary status of the active star PZ Mon

Yu. V. Pakhomov,¹ N. N. Chugai,¹ N. I. Bondar,² N. A. Gorynya,^{1,3} E. A. Semenko,⁴

¹*Institute of Astronomy, Russian Academy of Sciences, Pyatnitskaya 48, 119017, Moscow, Russia*

²*Crimean Astrophysical Observatory, Nauchny, Crimea, 2984009, Russia*

³*Lomonosov Moscow State University, Sternberg Astronomical Institute, Universitetskij prospekt, 13, Moscow 119991, Russia*

⁴*Special Astrophysical Observatory of Russian Academy of Sciences, Russia*

1 October 2014

ABSTRACT

We use original spectra and available photometric data to recover parameters of the stellar atmosphere of PZ Mon, formerly referred as an active red dwarf. The derived effective temperature $T_{eff}=4700$ K and gravity $\log g=2.8$ suggest that PZ Mon is a K2III giant. Stellar atmosphere parameters (T_{eff} and $\log g$) alongside with the evolutionary tracks are used to estimate the stellar mass of $\approx 1.5 M_{\odot}$ and the radius of $\approx 7.7 R_{\odot}$. The angular radius derived by the infrared flux method when combined with the linear radius suggests the distance of 250 ± 70 pc, a factor 2.5 smaller than that suggested by the *Hipparcos* parallax. The red giant status of PZ Mon is confirmed by the carbon and nitrogen abundance. The spectrum reveals pronounced He I 5876 Å absorption and H α emission indicating the robust chromosphere. The *IUE* spectrum is found to contain transition layer emission line of C IV 1550 Å. The C IV and X-ray luminosities turn out typical of RS CVn stars. The extended set of available photometric data confirms the period of 34.14 days presumably related to the stellar rotation. We found variations of the radial velocity with the amplitude of $\approx 8 \text{ km s}^{-1}$ which could be caused by the orbital motion.

Key words: stars: evolution – stars: fundamental parameters – stars: individual: PZ Mon – stars: variables: general

1 INTRODUCTION

PZ Mon (HD 289114, $V \approx 9$ mag) is K2Ve star rapid irregular variable of F-M/Fe-Me type (Samus et al. 2009) (see also SIMBAD). Now this classification seems an obsolete which reflects the history of PZ Mon study rather than the present day situation. First, however, we have to recap major observational facts. Pronounced variable Ca II and hydrogen emissions were found in several spectra taken between 1948 and 1954 which has prompted to classify PZ Mon as a flare K2-dwarf at the distance of ~ 30 pc (Münch & Münch 1955). The light curve of PZ Mon recovered from Harward archive between 1899 and 1954 demonstrated flare-type variations (Gaposchkin 1955) although it was stressed that the star had the relatively high visible magnitude for variables of this class. Later on PZ Mon was referred to as UV Cet type star (Petit 1958; Gershberg et al. 1999), although attribution to RW Aur type was suggested as well (Artiukhina 1959). The first distance estimate (30 pc) has been reduced to 16–21 pc (Gliese 1982; Stobie et al. 1989) with the lower limit preferred by Gershberg et al. (1999).

The compiled light curve of PZ Mon on the interval of 90 yr recovered from archive plates (Bondar’ 1995) shows long-term variations with the total B amplitude ~ 0.8 mag and the possible period of ~ 50 yr. These vari-

ations have been interpreted as a result of the activity of a spotted red dwarf (Bondar 1996; Alekseev & Bondar’ 2006). PZ Mon shows also short-term flux variations with the total amplitude ≈ 0.04 mag and period of about 34 d (Bondar & Prokof’eva 2007); they were attributed to the rotational flux modulation of the spotty star with the rotation period of 34 d.

The new history starts with the *Hipparcos* parallax data which suggested the distance of 1.4 kpc and the absolute magnitude $M_V \approx 0.2$ mag (Saar 1998). This combined with the known X-ray flux (Agrawal et al. 1986) prompted to make an assumption that PZ Mon is an active giant, probably of RS CVn type (Saar 1998). To support the giant status Saar (1998) compared the spectrum of PZ Mon with the red dwarf (HD 32147, K4V) and RS CVn type giant λ And (G8III-IV) and concluded that the giant matched better. However, later on it became clear that metallicity of both comparison stars was essentially non-solar: HD 32147 has enhanced metallicity ($[\text{Fe}/\text{H}] \approx 0.2 \dots 0.3$, Prugniel et al. 2011; Maldonado et al. 2012) while λ And is metal poor ($[\text{Fe}/\text{H}] = -0.56$, Massarotti et al. 2008). These facts weaken spectral arguments in favour of giant status of PZ Mon.

The change in the PZ Mon status raises several urgent questions: 1) Whether PZ Mon is a giant from the

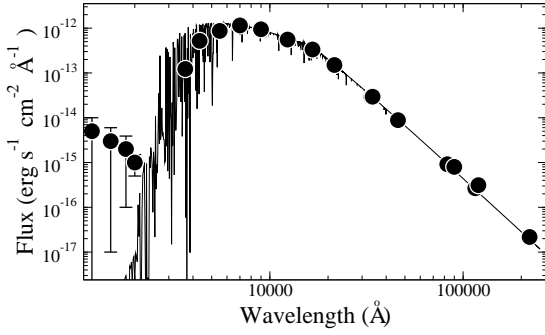


Figure 1. Spectral energy distribution of PZ Mon (dots) with the overplotted best fit model (line).

spectroscopic point of view? 2) If does, what are the stellar parameters and distance to PZ Mon? 3) Whether the chromosphere and corona are typical to active red giants of RS CVn type? 4) Are there any evidence that PZ Mon is a binary? The point is that even the revised *Hipparcos* parallax ($\pi = 1.57 \pm 1.01$ mas) (van Leeuwen 2007), with the distance of 640^{+1150}_{-250} pc – lower than adopted by Saar (1998) – admits a broad range of the luminosities. The answer to the posed questions constitute the subject of the present paper. Our motivation is also strengthened by the fact that PZ Mon has the longest (over 100 yr) record of the photometric variability with the large amplitude (~ 0.8 mag) of the long-term variation among RS CVn stars.

Below we address the PZ Mon status issue concentrating on the detailed analysis of the spectral and photometric data. Bearing in mind that PZ Mon might be a binary (Saar 1998) we explore also the radial velocity variations. In Sec. 2 we analyse photometric data to determine the effective temperature and the angular radius and study the photometric variability using more extended photometric set than before. In Sec. 3 the spectrum of PZ Mon will be analysed and parameters of stellar atmosphere and elemental abundances will be recovered. We then use the effective temperature and gravity alongside with evolutionary tracks to obtain the stellar parameters, specifically, mass, radius, luminosity, and distance (Sec. 4). In Sec. 5 we consider signatures of the chromosphere in the optical and *IUE* spectra and then finally discuss the nature of PZ Mon.

2 PHOTOMETRY

2.1 Effective temperature

Photometric data in *UBVRI* Johnson-Cousins system (Aleksiev & Bondar’ 2006) show variability of PZ Mon during 1992–2004 with the amplitude of 0.2–0.3 mag on the time scale of the hundreds days. The average color indices are $U - B = 1.05 \pm 0.04$ mag, $B - V = 1.17 \pm 0.02$ mag, $V - R = 1.18 \pm 0.02$ mag, $V - I = 1.73 \pm 0.03$ mag. The IR color indices are $V - J = 2.25 \pm 0.03$ mag, $V - H = 2.83 \pm 0.03$ mag, $V - K = 2.99 \pm 0.03$ mag, and $V - L = 3.03 \pm 0.04$ mag (Morel & Magnenat 1978; Cutri et al. 2003). We used a grid of synthetic colors (Castelli & Kurucz 2003) to find the best fit of all the available colors with the interstellar reddening taken into account according to Mathis (1990). The best fit at the 3σ level is found for two temperatures

Table 1. Effective temperature and angular diameter of PZ Mon derived from the photometric data by infrared flux method.

$E(B-V)$	T_{eff} , K	θ , mas
0.00	4640 ± 80	0.28 ± 0.01
0.03	4670 ± 80	0.28 ± 0.01
0.06	4700 ± 80	0.28 ± 0.01
0.10	4750 ± 80	0.29 ± 0.01

$T_{eff} = 4500$ K with $E(B - V) = 0.09$ mag, and $T_{eff} = 4750$ K with $E(B - V) = 0.19$ mag.

The infrared flux method (IRFM) (Blackwell & Shallis 1977) permits us to determine the angular diameter and the effective temperature in a more reliable way. The empirical spectral energy distribution of PZ Mon is recovered combining UV flux from *IUE* data (Wamsteker et al. 2000), optical flux from the *UBVRI* photometry, and near IR *2MASS* data (Cutri et al. 2003). We use also far IR flux of 0.2159 ± 0.00892 Jy at 9μ from the ARARI survey (Ishihara et al. 2010), 8.28μ flux of 0.2093 Jy (Egan et al. 2003), 12μ flux of 0.15 Jy (Gershberg et al. 1999), and IR fluxes from WISE mission (Wright et al. 2010): $W1(3.35\mu) = 6.177 \pm 0.088$ mag, $W2(4.6\mu) = 6.078 \pm 0.036$ mag, $W3(11.6\mu) = 6.073 \pm 0.015$ mag, and $W4(22.1\mu) = 5.927 \pm 0.046$ mag. The IR fluxes are only weekly affected by the reddening and temperature, which make them good indicators of the angular diameter $\theta = 2(f_{\lambda}^{obs}/F_{\lambda})^{1/2}$, where f_{λ}^{obs} is the observed flux and F_{λ} is the flux at the stellar photosphere. We proceed in a standard way using the iteration procedure and first guess for T_{eff} . The theoretical spectrum (Castelli & Kurucz 2003) for the adopted first guess $T_{eff} = 4700$ K is used to derive θ . This value and the integrated observed flux F is used to obtain new T_{eff} value from the relation $T_{eff} = (4F/\theta^2\sigma)^{1/4}$, where σ is the Stefan-Boltzmann constant. The iterations are repeated until the convergence. The spectral energy distribution for Kurucz model with $T_{eff} = 4700$ K and $E(B - V) = 0.06$ mag is shown in Fig. 1. The UV flux with high brightness temperature is strongly enhanced compared to the photospheric flux and undoubtedly is due to chromosphere of PZ Mon. The results of the T_{eff} determination by IRFM are shown in Table 2.1. Starting from the first column the table gives adopted reddening, effective temperature, and angular diameter. We made an attempt to derive the reddening in the framework of IRFM but found that this procedure was not unequivocal. We therefore show the temperature estimates for the several reddening values. The preferred value $E(B - V) = 0.06$ mag is determined by the equality between T_{eff} inferred by IRFM and spectroscopic method. Remarkably, the angular diameter is insensitive to the choice of the reddening.

2.2 Photometric variability

The extended set of ASAS-3 data (Pojmanski 1997, <http://www.astrouw.edu.pl/asas/>) between 2001 and 2009 is used to study the PZ Mon variability (Fig. 2). The reported data uncertainty is about 0.04 mag, although the actual error seems to be somewhat smaller. Indeed, the

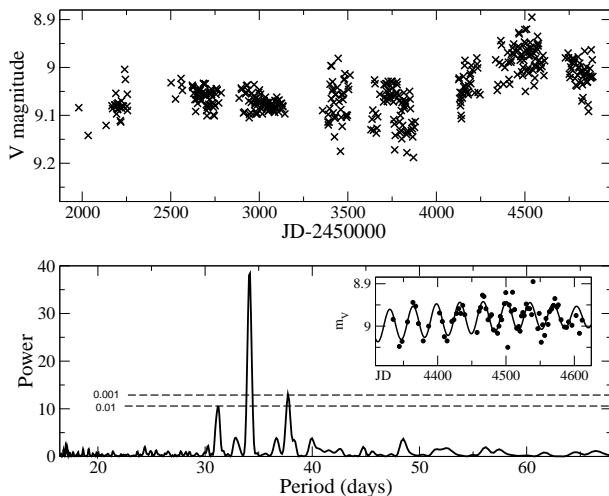


Figure 2. Light curve of PZ Mon according to ASAS-3 data (*upper panel*) and power spectrum of the Lomb periodogram (*lower panel*). Horizontal lines show the significance levels. The *inset* shows a fragment of the ASAS-3 data record with overlaid 34.14 d oscillations.

flux variation during JD 2454335–2454611 (Aug 2007 – May 2008) shows the apparent periodic signal with the amplitude of ≈ 0.05 mag and period of about 34 d (Fig. 2, inset). We analyzed all the available data sets by the Lomb method to recover significant peak in the periodogram (Fig. 2) at 34.14 days. Two smaller side peaks have caused by the gaps in the data set. The found period well coincides with the period value obtained earlier (Bondar & Prokof'eva 2007) and identified with the rotational period.

3 SPECTROSCOPY

3.1 Observations and spectrum overview

Two spectra of PZ Mon were obtained 2012 November 4/5 with NES2 echelle spectrograph installed in Nasmyth focus at 6-m telescope of Special Astrophysical Observatory of Russian Academy of Sciences. Two one hour exposures were taken on CCD (2068x4632) starting at 2012 Nov. 4 22:45 UT and 2012 Nov. 5 01:50 UT respectively. Data have been reduced using MIDAS package ECHELLE. Fifty echelle orders were extracted in the region of 4080 – 7181 Å with the wavelengths calibrated via ThAr hollow-cathode lamp. The spectra normalization was performed with the blaze function obtained from flat field exposures. Two spectra of PZ Mon were combined together with the allowance for the Earth rotation. The average signal-to-noise ratio of the resulting spectrum ranges from 25 in the blue to 110 in the red.

At first glance the spectrum of PZ Mon is typical for normal early K-stars. Closer inspection shows however that there is a signature of the emission in the blue part of the H α profile. Moreover, usually strong absorptions in K-stars (hydrogen lines, MgI 5170 Å, and NaI 5890 Å) turn out to be not so deep compared to normal red stars of similar temperature. The spectrum also reveals HeI 5876 Å (D₃) absorption that suggests the presence of the pronounced chromosphere with the transition layer where the helium should be excited.

Chromospheric effects are likely responsible also for the relatively high central intensity of strong absorption lines.

We do not confirm the presence of molecular features of TiO at 4760 Å and 4950 Å as well as MgH at 4780 Å reported earlier (Pettersen & Hawley 1989) which were the result of misinterpretation. The spectrum synthesis reveals the atomic lines blends. We convolved our spectrum with the Gaussian corresponding to the resolution of $R=1200$ in order to compare PZ Mon spectrum with the spectrum of Pettersen & Hawley (1989) and found no difference in the range of 4080–4960 Å. Molecular line of TiO at 7055 Å known as indicator of cool stellar spots is absent. The spectrum in this region is essentially similar to those of normal red giants.

The radial velocity derived from our spectrum is 27.3 ± 0.4 km s⁻¹, a slightly lower than 28.9 ± 0.3 km s⁻¹ reported by Saar (1998). The straightforward explanation of the difference might be a binary nature of PZ Mon. Yet we did not find any signature of the secondary component in the PZ Mon spectrum.

3.2 Galactic kinematics and metallicity

The Hipparcos parallax of PZ Mon (van Leeuwen 2007) implies the distance of 640^{+1150}_{-250} pc. This distance when combined with the *Hipparcos* proper motion and the radial velocity implies the galactic velocity components (U, V, W) = $(17 \pm 3, 227 \pm 5, -18 \pm 17)$ km s⁻¹. The galactic latitude of PZ Mon is $-0^\circ.131$. This fact combined with U, V, W velocity components imply that PZ Mon has almost galactic orbit in the galactic plane close to the solar galactic radius. We conclude therefore that the metallicity of PZ Mon should not differ significantly from solar. We therefore assume the solar metallicity of PZ Mon; this assumption will be confirmed below by the detailed spectral analysis.

3.3 Parameters of stellar atmosphere

The rotation velocity derived from several unblended lines using BINMAG3 code¹ is $v \sin i = 10.5 \pm 0.6$ km s⁻¹, very much close to 10.2 ± 0.4 km s⁻¹ found earlier (Saar 1998). This value exceeds the typical rotational velocity of normal red giants but is consistent with the fast rotation of active stars (Gondoin 2007; Oláh et al. 2013). The macroturbulent velocity derived from profile analysis of 27 unblended line of FeI, TiI, and NiI is $v_{\text{macro}} = 5.2 \pm 0.5$ km s⁻¹ consistent with 5.5 ± 0.8 km s⁻¹ reported by Saar (1998), large for red dwarfs but typical to red giants (Gray 1982, 1984).

A standard prescription for the determination of the effective temperature makes use of the requirement that the iron abundance derived from FeI lines should not depend on the excitation potential (E). We selected 34 lines of FeI with the equivalent width of 30–110 mÅ and excitation potential of $0.91 < E < 4.99$ eV in the range of 5200–6700 Å; this range permits us to avoid strong molecular lines, telluric lines, and fringes. In the abundance determination we exploit WIDTH9 code written by V. Tsymbal on the bases of the R. Kurucz code. Atomic and molecular data are extracted from VALD3 database (Ryabchikova et al. 2011).

¹ <http://www.astro.uu.se/~oleg/binmag.html>

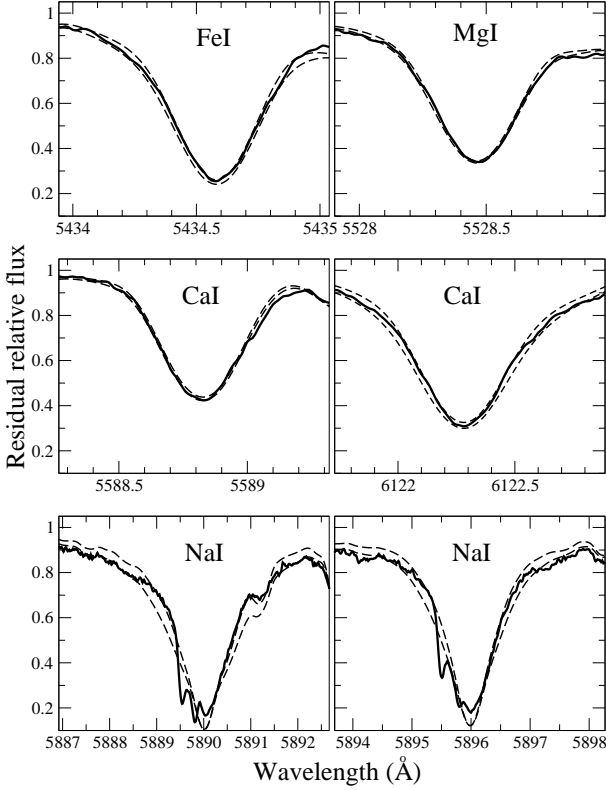


Figure 3. Observed lines of several neutrals (*solid line*) compared to the model spectra (*dashed*). For every profile we show two models which correspond to the $\log g$ value that differ from the optimal by ± 0.2 .

Table 2. The parameters of strong spectral lines and the gravity estimation.

λ Å	Ion	E eV	$\log gf$	$\log \Gamma_r$ s^{-1}	$\log \frac{\Gamma_S}{N_e}$ s^{-1}	$\log \frac{\Gamma_W}{N_H}$ s^{-1}	$\log g$
5434.5	FeI	1.011	-2.122	7.140	-6.220	-7.749	2.93 ± 0.11
5528.4	MgI	4.346	-0.498	8.720	-4.460	-6.979	2.47 ± 0.18
5588.8	CaI	2.526	0.358	7.853	-6.072	-7.538	2.68 ± 0.19
6122.2	CaI	1.886	-0.316	7.860	-5.320	-7.189	2.75 ± 0.19
5889.9	NaI	0.000	0.108	7.799	-5.640	-7.526	2.93 ± 0.18
5895.9	NaI	0.000	-0.194	7.798	-5.640	-7.526	2.87 ± 0.15

We derived the microturbulent velocity 1.4 km s^{-1} using the standard requirement that the Fe/H ratio should not depend on the FeI line intensity. As a result we find the effective temperature $T_{eff} = 4700 \pm 100 \text{ K}$ and the iron abundance of $[\text{Fe}/\text{H}] = 0.0 \pm 0.1$. The surface gravity $\log g = 2.9 \pm 0.2$ is estimated from the profile fit of FeII unblended lines 5425.26, 6149.24, 6432.68, 6456.39 Å using BINMAG3 code.

The independent diagnostics of gravity is provided by wings of strong spectral lines. We selected four unblended lines of FeI, MgI, and CaI with the residual flux of < 0.4 and applied SYNTHV code (Tsymbal et al. 2003) adopting $T_{eff} = 4700 \text{ K}$ to model the line profiles adopting (Fig. 3). The gravity $\log g$ is derived for every pixel and the final value is obtained as the average for each line and presented in last column of Table 2. The table includes also atomic parameters (Kupka et al. 1999), viz., wavelength, ion, exci-

tation potential of the lower level, oscillator strength, radiation damping constant, Stark and van der Waals broadening parameters calculated for 10 000 K.

In case of NaI D₁ and D₂ we unable to fit the whole profile because cores of these lines are affected by the chromosphere. We therefore concentrated on the wings with the residual intensity > 0.3 in the regions without the interstellar lines. The $\log g$ values derived from NaI lines (Table 2) agree with the $\log g$ derived from other neutrals and all these values are consistent with $\log g$ inferred from FeII lines. The overall average value is $\log g = 2.8 \pm 0.2$. The effective temperature $T_{eff} = 4700 \pm 100 \text{ K}$ and gravity $\log g = 2.8 \pm 0.2$ suggests that PZ Mon should be classified as K2III giant.

3.4 Abundance of C, N, and Li

Generally red giants show underabundance of carbon and overabundance of nitrogen caused by the first dredge-up of products of CNO cycle (Lambert & Ries 1981). The of CNO elements therefore can be an independent signature of a red giant nature of PZ Mon. The LTE BINMAG3 code is used to determine the C and N abundance of PZ Mon. We adopt parameters derived above ($T_{eff} = 4700$, $\log g = 2.8$, and $V_t = 1.4 \text{ km s}^{-1}$) and atomic/molecular data from VALD3 database (Ryabchikova et al. 2011). Analysis of molecular lines of C₂ at 5086 Å and 5135 Å, which are sensitive to the carbon abundance, results in $[\text{C}/\text{H}] = -0.1 \pm 0.1$. Molecular lines of CH at 4835 Å indicate somewhat larger underabundance $[\text{C}/\text{H}] = -0.4 \pm 0.2$. The nitrogen abundance inferred from CN molecular lines at 6250–6251 Å is $[\text{N}/\text{H}] = 0.15 \pm 0.20$. The slight underabundance of carbon and overabundance of nitrogen with respect to the solar composition are marginally consistent with the effect of the first dredge-up and therefore are in line with the giant status of PZ Mon.

The Li abundance in giants shows large scatter with $A(\text{Li}) = \log(\text{Li}/\text{H}) - 12 \sim -1 \dots 2.8$ in the range of $T_{eff} \sim 4400\text{--}5000 \text{ K}$ (Palmerini et al. 2011) although the bulk of giants has $A(\text{Li}) < 1.5$ and only 2% have $A(\text{Li}) \geq 1.5$ (Brown et al. 1989). In PZ Mon the Li 6707 Å line is rather pronounced. The contribution of blending lines of CN, CeII, SmII, FeI, and V_I is small (Fig. 4). To derive the lithium abundance we use BINMAG3 code. The hyperfine splitting and other atomic and molecular line contributions are taken into account with the atomic data from VALD3. The resulting of LTE lithium abundance is $A(\text{Li}) = 1.50 \pm 0.05$. Using a grid of non-LTE calculations from (Lind et al. 2009) we recover the non-LTE correction $A_{nLTE} - A_{LTE} = +0.19 \text{ dex}$, so the corrected Li abundance is $A(\text{Li}) = 1.69 \pm 0.05$. For consistency we compare our LTE result with available LTE data. The value $A(\text{Li}) = 1.5$ turns out at the boundary between giants with relatively high Li abundance ($A(\text{Li}) \geq 1.5$) and normal K-giants ($A(\text{Li}) < 1.5$).

3.5 Variation of radial velocity

Only one measurement of the PZ Mon radial velocity (RV) has been made formerly (Saar 1998) (#1 in Table 3). Table columns give the order number of the observational set, Julian day, radial velocity v_{rad} and the errors. The bulk of data (sets #2 and #4) we obtained using Radial Velocity Meter

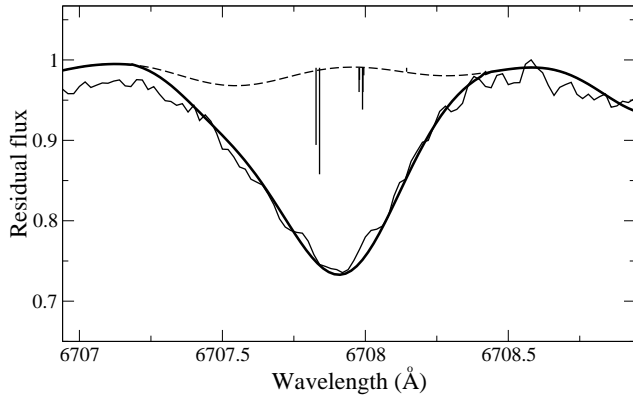


Figure 4. LiI 6707 Å in the spectrum of PZ Mon (*thin* line). The synthetic spectrum is shown by *thick solid* line. The synthetic spectrum without LiI line is shown by *dashed* line. The positions of lithium doublet components with hyperfine splitting are shown by vertical lines.

Table 3. Radial velocity of PZ Mon.

Set	JD	v_{rad} km s ⁻¹	σv_{rad} km s ⁻¹
1	2447834.997	28.9	0.3
2	2455860.607	29.58	0.22
	2455861.620	28.94	0.28
3	2456235.375	27.3	0.4
4	2456598.584	24.18	0.23
	2456602.597	28.35	0.30
	2456603.545	29.09	0.27
	2456604.639	29.28	0.34
	2456605.709	29.36	0.29
	2456606.609	30.72	0.24
	2456607.613	31.98	0.28
	2456611.558	29.14	0.28
	2456612.592	29.05	0.37
5	2456694.322	32.3	1.0

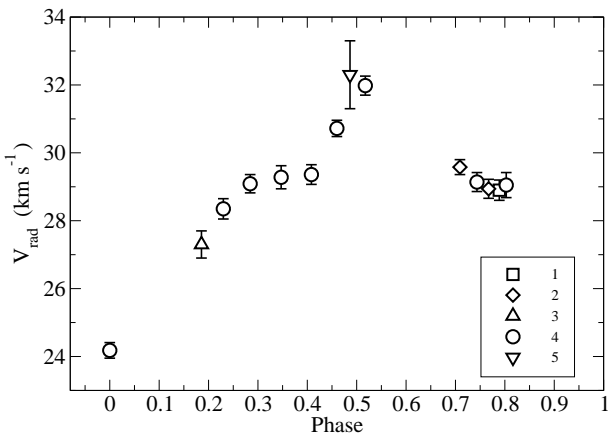


Figure 5. The radial velocity measurements convolved with period $P=17.45$ d. Different sets (Table 3) are shown by different symbols.

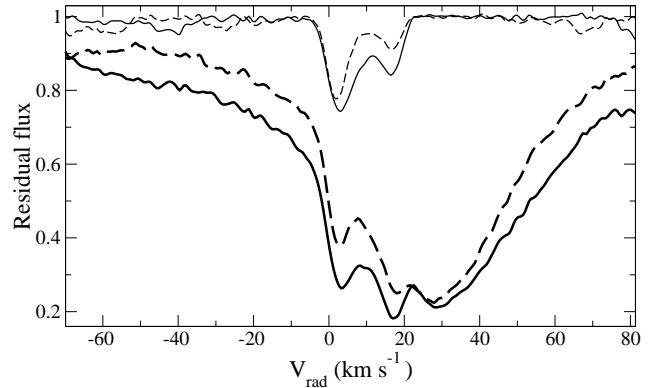


Figure 6. Sodium D₁ (*thick dashed* line) and D₂ (*thick solid*) in the spectrum of PZ Mon and extracted interstellar lines (*thin* lines).

(RVM) (Tokovinin 1987) installed at the Simeiz 1-m telescope of the Crimean Astrophysical Observatory. Zero point velocity was determined by observations of several IAU velocity standards each night. The #3 value was described in Sec. 3.1. One point (#5) was taken 2014 Feb. 5 using MMSC echelle spectrograph ($R=13000$) at the 2-m telescope Zeiss-2000 of the Terskol Observatory of Institute of Astronomy of Russian Academy of Sciences.

Radial velocities of the major set #4 show rise and fall of velocity between 24 km s^{-1} and 32 km s^{-1} with the maximum at about JD 2456607.6. Remarkably, the velocity at JD 2456694.3, i.e., 86.7 d later (set #5) $\approx 32 \text{ km s}^{-1}$ is similar to the maximum value. This leads to assumption that RV variations of PZ Mon are periodic, 86.7 d is an interval which consists of the integer number of periods. We explored all possible periods in the range of $P \leq 90$ days and find only one optimum value $P=17.45$ d ($\approx (1/5)86.7$ d) which provides the best fit for the folded data on the phase RV curve (Fig. 5). This result indicates that the PZ Mon radial velocity possibly varies periodically.

4 PZ Mon DISTANCE

4.1 Interstellar absorptions

The spectrum shows pronounced interstellar NaI D₁ and D₂ absorptions (Fig. 6) which can be distance indicators. To extract the interstellar NaI lines we apply the mirror transform of red wing of the stellar line with the control by synthetic spectrum. The extracted interstellar lines are shown in Fig. 6. The absorption shows two components, A at 3.2 km s^{-1} and B at 17.5 km s^{-1} . The A component with the equivalent widths of $36.2 \pm 2 \text{ mÅ}$ and $28.5 \pm 2 \text{ mÅ}$ in D₂ and D₁ lines respectively is obviously saturated, while the B component with the equivalent widths of $20.4 \pm 2 \text{ mÅ}$ and $11.0 \pm 2 \text{ mÅ}$ is far from the saturation. We use both of doublet components which makes the inferred column density and broadening parameter more reliable (cf. Pakhomov et al. 2012). The derived column density and broadening parameter for A component are $N(\text{NaI}) = (9 \pm 2) \times 10^{11} \text{ cm}^{-2}$ and $b = 0.5 \text{ km s}^{-1}$ respectively, while for B component $N(\text{NaI}) = (1.1 \pm 0.1) \times 10^{11} \text{ cm}^{-2}$ and $b = 1.0 \text{ km s}^{-1}$.

The local interstellar medium is known to have of a low density and referred to as local bubble with the radius of $\sim 100 - 150$ pc (Welsh et al. 2010). All sky survey of the NaI interstellar absorption (Welsh et al. 1998) shows that towards the stars with distances $d < 50$ pc the NaI interstellar absorption is very weak with $\log N(\text{NaI}) < 11.0$. The presence in the PZ Mon spectrum of NaI interstellar absorptions with $N(\text{NaI}) = (9 \pm 2) \times 10^{11} \text{ cm}^{-2}$ therefore implies the distance to PZ Mon of > 50 pc. This disfavors the red dwarf status for PZ Mon in accord with the K2III classification based on the spectral analysis.

4.2 Stellar parameters and distance

The derived stellar atmosphere parameters $T_{\text{eff}} = 4700 \pm 100$ K and gravity $\log g = 2.8 \pm 0.2$ can be combined with stellar evolutionary tracks to estimate the mass. We employ evolutionary tracks (Girardi et al. 2000) for the metallicity $Z = 0.019$ to find $M = 1.5 \pm 0.5 M_{\odot}$. This value alongside with $\log g$ immediately provides us with the stellar radius of $R = 7.7 \pm 2 R_{\odot}$. The radius and T_{eff} imply the bolometric luminosity of $\log L/L_{\odot} = 1.4 \pm 0.3$. For given T_{eff} , $\log g$, and $B - V$ the Kurucz models permits us to estimate the reddening $E(B - V) = 0.08 \pm 0.02$ mag that agree with value of 0.06 mag derived from IRFM. The angular diameter (0.28 ± 0.01 mas) combined with the linear radius gives the estimation of distance $d = 250 \pm 70$ pc (or parallax $\pi = 4.0 \pm 1.1$ mas). This value is by factor 2.5 lower than distance estimated from *Hipparcos* parallax (640 pc).

5 CHROMOSPHERE SIGNATURES

The spectrum of PZ Mon shows the $\text{H}\alpha$ emission component presumably related to the chromosphere. In Fig. 7 the PZ Mon spectrum in the $\text{H}\alpha$ band is shown alongside with the spectra of two normal red giants with similar parameters: HD24758 ($T_{\text{eff}} = 4680$ K, $\log g = 2.75$, $[\text{Fe}/\text{H}] = 0.11$) and HD184423 ($T_{\text{eff}} = 4680$ K, $\log g = 2.85$, $[\text{Fe}/\text{H}] = 0.12$) (Pakhomov et al. 2011; Pakhomov 2013). Both comparison spectra were broadened with the rotation velocity of PZ Mon (10.5 km s^{-1}); telluric lines were removed from all the spectra. Note that weak spectral lines in all three spectra are similar, while the $\text{H}\alpha$ of PZ Mon is very much different: the absorption is shallow and in blue wing the emission excess is apparent. The difference between the PZ Mon spectrum and average spectrum of the two other giants is shown in Fig. 7 (bottom panel). The monochromatic luminosity scale corresponds to $d = 250$ pc and $E(B - V) = 0.06$ mag.

The residual $\text{H}\alpha$ emission consists of the central component with the luminosity of $5.5 \times 10^{30} \text{ erg s}^{-1}$ and broad component composed of the blueshifted and redshifted emissions with the total luminosity of $4.5 \times 10^{30} \text{ erg s}^{-1}$. The overall $\text{H}\alpha$ luminosity (narrow + broad emission) is $\approx 10^{31} \text{ erg s}^{-1}$, which corresponds to $\approx 10^{-4}$ of the PZ Mon bolometric luminosity. We decompose the residual $\text{H}\alpha$ profile into three components: narrow emission with FWHM $\approx 50 \text{ km s}^{-1}$ redshifted relative to photospheric spectrum by 5 km s^{-1} , broad emission with FWHM $\approx 170 \text{ km s}^{-1}$ blueshifted by -40 km s^{-1} , and the central saturated shallow absorption

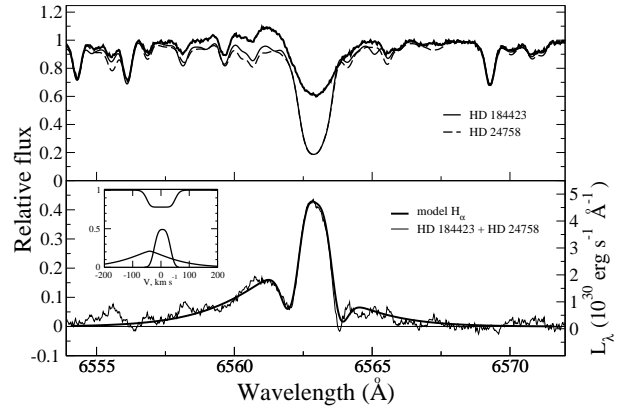


Figure 7. $\text{H}\alpha$ profile in the spectrum of PZ Mon (thick solid line) compared to spectra of HD24758 and HD184423 (top panel). Lower pane: The average residual (thin line) and model (thick). Inset shows model components.

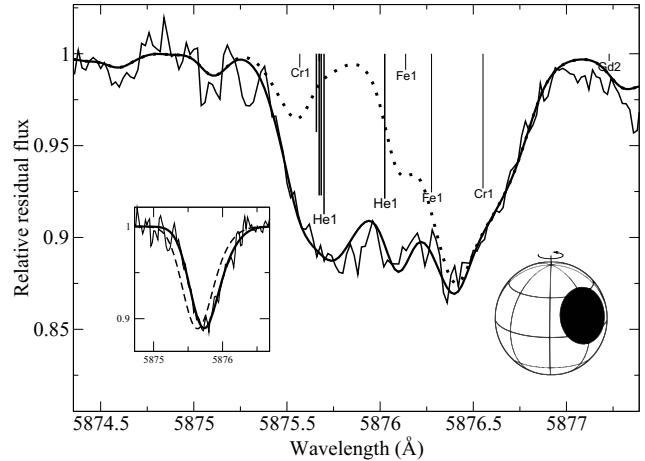


Figure 8. He I 5876 Å in the spectrum of PZ Mon (thin line). Synthetic spectrum is shown by thick solid line. Dotted line shows synthetic spectrum without He I 5876 Å. Inset shows the residual spectrum (thin line) and model spectrum without spot (dashed line) and with the spot (solid line). The spot configuration is rendered in the drawing (right bottom).

(Fig. 7, inset). The latter can be described by the Gaussian absorption profile with the broadening of 32 km s^{-1} , the central optical depth of $\tau_0 = 9$, and stellar surface covering factor of 0.22. This absorption is presumably related to enhanced hydrogen excitation in the patchy chromospheric structure. The narrow $\text{H}\alpha$ emission arises in the chromospheric plagues likewise in RS CVn stars (Biazzo et al. 2006). The origin of the broad $\text{H}\alpha$ component which is usually seen in RS CVn stars is an unsettled issue. It probably originates from flaring activity (Montes et al. 1997), although the corotating emission region or wind are proposed as well (Hatzes 1995).

5.1 He I 5876 Å absorption

The He I 5876 Å absorption is a major component of the absorption feature in the range 5875.3–5876.2 Å (Fig. 8). The He I 5876 Å absorption is commonly seen in spectra

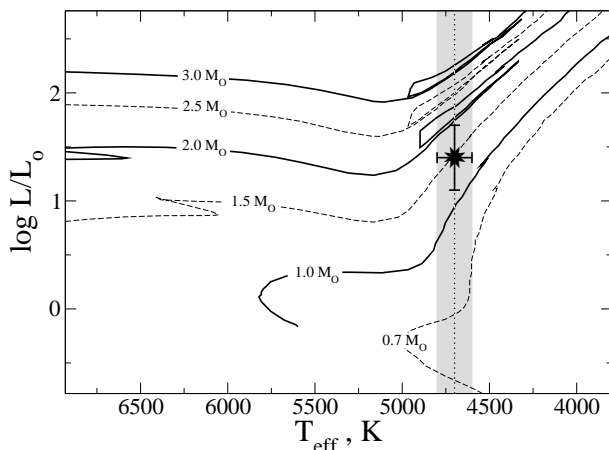


Figure 9. HR diagram with the PZ Mon shown by star symbol. The range of temperature of PZ Mon is marked by *gray strip*.

of active stars both dwarfs (Saar et al. 1997) and giants (Montes et al. 1997). In the cool active star the helium line could form only in the upper chromosphere. We recover the contribution of HeI absorption as a residual from the ratio of the observed spectrum to the synthetic spectrum of PZ Mon (Fig. 8, inset). The HeI absorption is redshifted by 4.5 km s^{-1} relative to photospheric spectrum. Remarkably, this redshift is similar to that of the narrow H α emission component (5 km s^{-1}) which suggests that both lines form probably in the same large active region.

The HeI 5876 Å redshift can be explained in the model of a large spot of the excited HeI on the rotating star with the spot approaching the limb. For the circular spot on a star with the inclination of the rotational axis $i = 70^\circ$ and rotational velocity of 11.4 km s^{-1} the optimal parameters choice suggests the spot radius of 33.5° with the spot center at the longitude of 43° relative to the central meridian and the latitude of 20° counted from the rotational equator toward the “visible” pole (Fig. 8, inset). The adopted microturbulent velocity is 8 km s^{-1} and the macroturbulent is 10 km s^{-1} . The limb darkening is treated in the first Chandrasekhar approximation ($I(\theta) \propto 1/\sqrt{3} + \cos \theta$). The model requires that the contribution of the rest of the stellar disk in the HeI 5876 Å absorption should not exceed 2%. The direct test of the spot model for the HeI 5876 Å would be the detection of the variable line shift with rotational phase.

6 DISCUSSION

Our primary goal was to establish the evolutionary status of PZ Mon on the bases of the detailed photometric and spectral analysis. We inferred the effective temperature and gravity which indicate that PZ Mon is K2III giant. In combination with the stellar evolutionary tracks the effective temperature and gravity suggest the mass of PZ Mon of $\approx 1.5 M_\odot$. This in turn permitted us to infer the radius, luminosity, and the distance of PZ Mon; the latter estimate is based on the stellar angular radius recovered by IRFM. The star resides in the red giant branch of the HR diagram (Fig. 9).

Basically the presence of cool spots distorts the SED so the temperature determined above by three methods should

contain errors. Unfortunately, there is no photometric data coeval with spectral ones. In order to estimate the spottedness effects we therefore adopt the background stellar temperature of 4750 K and consider spots with the covering factor of 0.3 estimated by Alekseev & Bondar’ (2006). The spot temperature is assumed to be in the range of 3500–4500 K. The fluxes are taken from the grid of models by Castelli & Kurucz (2003). The maximum change of $(B - V)$ color caused by the spottedness ($+0.03 \text{ mag}$) is attained for $T_{\text{spot}} = 4000 \text{ K}$ which results in the reduction of the temperature by 83 K, i.e., within errors. The infrared fluxes of spotted star are reduced by the factor of 0.9 so the angular diameter and the distance determined by IRFM turn out larger by 5%, also within errors. In this case the new temperature is 4640 K, i.e., within errors. The temperature derived from FeI lines is least sensitive to the stellar spottedness decreasing only by 64 K. To summarize, the effective temperature of PZ Mon may be in the range of 4700–4800 K with the error about 100 K. The reddening derived in Section 4.2 (0.08 ± 0.02) is reduced for the spotty model to $E(B - V) = 0.06 \pm 0.03$.

Our spectrum reveals signatures of the robust PZ Mon chromosphere demonstrated by the H α emission and HeI 5876 Å absorption. The H α emission apparently consists of two components: (i) narrow ($\text{FWHM} \approx 50 \text{ km s}^{-1}$) and (ii) the broad emission with $\text{FWHM} \approx 170 \text{ km s}^{-1}$ blueshifted by -40 km s^{-1} . This kind of H α profile with blueshifted broad component is rather common for active RS CVn-type giants, *viz.*, HK Lac (K0III), IM Peg (K2III) (Biazzo et al. 2006), DM UMa (Hatzes 1995). At present there is no unequivocal model for the broad component. The wind is unlikely because in this case the required emission measure can be attained only for the very high mass loss rate $\dot{M} \sim 7 \times 10^{-9} v_{200} M_\odot \text{ yr}^{-1}$ (where v_{200} is the wind velocity in units of 200 km s^{-1}). This is by a factor ~ 50 larger than the mass loss rate suggested by the modified Reimers law (Schröder & Cuntz 2005). The flaring activity accompanied by the high velocity ejecta is the likely explanation. The broad H α line-emitting sites in this scenario can be thought of as an analogue of the solar eruptive prominences. This scenario naturally accounts for the dominant blueshift of the broad component. Indeed, in this case we are able to account for both the variability of broad H α and the dominance of the blueshift due to the occultation effect.

We find it remarkable that the HeI 5876 Å absorption redshift (4.5 km s^{-1}) and the narrow H α emission (5 km s^{-1}) redshift are similar. We interpret this as an outcome of the spot on the rotating star in which case the HeI absorption and H α narrow emission form in similar region of the chromosphere. In fact, DM UMa (RS CVn type) shows synchronized rotational modulation of narrow H α and HeI D₃ (Hatzes 1995). In this respect a question arises, whether the active region responsible for H α and HeI D₃ is located over the photospheric spot responsible for the photometric variations. At the moment, simultaneous spectral and photometric observations are absent and this question cannot be answered. It is instructive to estimate the spot size and the spot temperature contrast required in order to account for the photometric variation of 0.07 mag. We consider two cases: dark spot and bright spot assuming the stellar temperature of 4700 K and the same spot radius 55° . We find

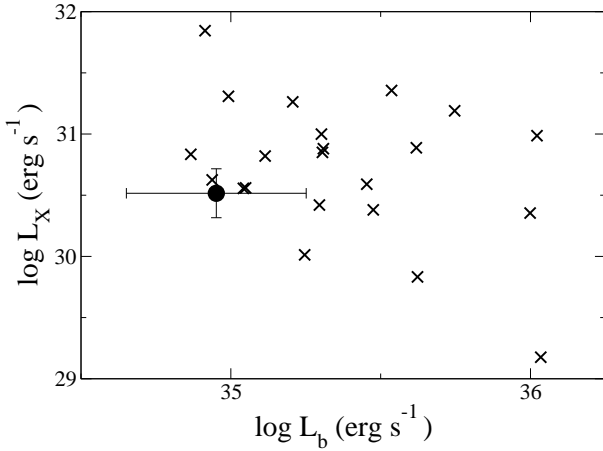


Figure 10. PZ Mon (dot with error bars) in the L_x vs. L_b scatter plot for active giants. Data are from (Gondoin 2007).

that the dark spot temperature should be 3800 K, while the bright spot 5200 K.

The archive *IUE* spectrum of PZ Mon (Wamsteker et al. 2000) reveals chromospheric lines of Mg II, O I, Si II, He II, and C IV (Table 6). The table contains also the observed integrated fluxes we recovered from the line luminosities corrected for the extinction. Although the chromospheric lines could be variable we note that the ratio of Mg II 2800/H α =1.3 is comparable to the solar ratio Mg II 2800/H α \approx 2 (Ulmschneider 1979). We find that C IV luminosity of PZ Mon $\log L(\text{C IV}) \approx 29.8$ (erg s^{-1}) is within the range 29.1–30.2 typical of RS CVn binaries (Dempsey et al. 1993).

With the new distance PZ Mon X-ray luminosity can be compared with other RS CVn stars. The *Einstein* count rate of PZ Mon X-ray flux is 0.014 ± 0.003 cts (McDowell 1994). To recover the X-ray unabsorbed flux we estimate the interstellar hydrogen column density from the correlation between N_H and A_V (Güver & Özel 2009), $N_H = 4 \times 10^{20} \text{ cm}^{-2}$, and from the correlation between N_H and $N(\text{Na I})$ (Ferlet et al. 1985), $N_H = 4.9 \times 10^{20} \text{ cm}^{-2}$. Both values are similar with the average of $N_H = 4.45 \times 10^{20} \text{ cm}^{-2}$. Adopting this value and the typical coronal temperature of 1 keV for RS CVn stars (e.g. Gondoin 2007) we find using HEASARC webPIMMS tools the unabsorbed flux of $(4.4 \pm 1.1) \times 10^{-13} \text{ erg cm}^{-2} \text{ s}^{-1}$ in 0.3–10 keV band. This corresponds to the X-ray luminosity $L_X = (3.3 \pm 2.1) \times 10^{30} (d/250\text{pc})^2 \text{ erg s}^{-1}$. The found value exceeds the X-ray luminosity of normal single red giants by a factor of $\sim 10^3$ (Schroeder et al. 1998). On the other hand, the X-ray luminosity of PZ Mon gets into the range $\log L_X \approx 29 - 32$ (erg s^{-1}) typical of active giants in binaries (Gondoin 2007) as demonstrated by the scatter diagram (Fig. 10). With regard to the X-ray luminosity PZ Mon turns out typical RS CVn type active giant. The attribution of PZ Mon to the RS CVn class has been first proposed by Saar (1998).

The classification of PZ Mon as RS CVn type star implies that the star could be a binary (Saar 1998). We found variations of the radial velocity, although the appearance of the radial velocity curve with the sharp maximum is unusual for RS CVn binaries. We therefore considered an alternative scenario: the rotational modulation due to the star

Table 4. Fluxes of emission lines in UV spectrum of PZ Mon.

λ Å	Ion	Flux $\text{erg cm}^{-2} \text{ s}^{-1}$	L_{line} erg s^{-1}	$\log \frac{L_{\text{line}}}{L_{\text{bol}}}$
1305	O I	6.1×10^{-14}	8.1×10^{29}	-5.1
1548	C IV	5.3×10^{-14}	6.4×10^{29}	-5.2
1640	He II	2.9×10^{-14}	3.5×10^{29}	-5.4
1815	Si II	2.8×10^{-14}	3.4×10^{29}	-5.5
2800	Mg II	1.2×10^{-12}	1.3×10^{31}	-3.9

spot. Assuming that the photometric period of 34.14 d is the rotational period the stellar radius of $7.7 R_{\odot}$ suggests the equatorial rotational velocity of $v = 11.4 \pm 3.0 \text{ km s}^{-1}$. With $v \sin i = 10.5 \text{ km s}^{-1}$ one finds then the inclination $\sin i = 0.92 \pm 0.25$. These parameters are used to find the optimal size of the spot assuming certain spot brightness contrast. It turns out that the model aimed to account for the required line shift predicts the photometric variability with the amplitude of ≈ 0.45 mag. This is at odds with the observed amplitude of only 0.07 mag. We therefore reject this scenario. Note however that this conclusion does not refer to the spot model for the redshift of chromospheric lines and spot model for the photometric variability.

We are left thus with the conjecture that the velocity variations are caused by the orbital motion probably with some effects of spot superimposed on the smooth curve. In that scenario the suggested orbital period is $P = 17.45$ d and the velocity amplitude of 3.9 km s^{-1} . Assuming zero eccentricity we come to the mass function $f(M_2) = (M_1 \sin i)^3 / (M_1 + M_2)^2 = 1.08 \times 10^{-4}$. With the inclination $0.67 < \sin i < 1$ and the primary mass of $M_1 = 1.5 M_{\odot}$ the mass function suggests the secondary mass of $0.064 < M_2 < 0.097 M_{\odot}$. This range is close to the brown dwarf limit ($\sim 0.075 M_{\odot}$) with little hope to detect the companion via the direct imaging (apparent magnitude ~ 27 mag). The only reasonable confirmation of the binary nature of PZ Mon will be the periodic radial velocity curve based on a more complete data set.

With the new classification PZ Mon reveals the new quality as the RS CVn variable with the longest photometric data set (~ 100 yr), the longest quasi-period of ~ 50 yr of activity and the largest amplitude of long-term variation ~ 0.8 mag among studied RS CVn stars.

7 CONCLUSIONS

The analysis of the photometric and spectral data leaves no doubt that the active red star PZ Mon is in fact an active K2III giant with the chromosphere and corona properties compatible with the typical RS CVn star. This makes PZ Mon the object of a special interest because a long available photometric set of data which shows the long-term variation of activity with the large amplitude. We conjecture that PZ Mon short-term variability with the period of 34.14 d is related to the large active spot on the rotating star. We found similar redshift of narrow H α emission and He I D₃ absorption which are likely related to the active spot on the rotating star. We found significant variations of the radial velocity which could be caused by the orbital motion.

ACKNOWLEDGMENTS

We are grateful to Ilya Sokolov for the spectral observation at Terskol observatory. This work is supported by the grant "Nonstationary Phenomena in the Universe" of the Russian Academy of Sciences. We thank the administration of the Simeiz Section of the Crimean Astrophysical Observatory for allocating observation time at the 1-m telescope. This work was partial supported by the Russian Foundation for Basic Research (projects 11-02-00608 and 14-02-91153).

REFERENCES

- Agrawal P. C., Rao A. R., Sreekantan B. V., 1986, *MNRAS*, 219, 225
- Alekseev I., Bondar' N., 2006, *Astronomical and Astrophysical Transactions*, 25, 247
- Artiukhina N. M., 1959, *Soviet Astronomy*, 3, 832
- Biazzo K., Frasca A., Catalano S., Marilli E., 2006, *A&A*, 446, 1129
- Blackwell D. E., Shallis M. J., 1977, *MNRAS*, 180, 177
- Bondar' N. I., 1995, *A&AS*, 111, 259
- Bondar N. I., 1996, *Bulletin Crimean Astrophysical Observatory*, 93, 95
- Bondar N. I., Prokof'eva V. V., 2007, *Odessa Astronomical Publications*, 20, 14
- Brown J. A., Sneden C., Lambert D. L., Dutchover Jr. E., 1989, *ApJS*, 71, 293
- Castelli F., Kurucz R. L., 2003, in Piskunov N., Weiss W. W., Gray D. F., eds, *Modelling of Stellar Atmospheres Vol. 210 of IAU Symposium, New Grids of ATLAS9 Model Atmospheres*. p. 20
- Cutri R. M., Skrutskie M. F., van Dyk S., et al., 2003, *2MASS All-Sky Catalog of Point Sources*, University of Massachusetts and Infrared Processing and Analysis Center, (IPAC/California Institute of Technology)
- Dempsey R. C., Linsky J. L., Schmitt J. H. M. M., Fleming T. A., 1993, *ApJ*, 413, 333
- Egan M. P., Price S. D., Kraemer K. E., et al., 2003, *MSX6C Infrared Point Source Catalog. The Midcourse Space Experiment Point Source Catalog Version 2.3* (October 2003). Air Force Research Laboratory Technical Report AFRL-VS-TR-2003-1589
- Ferlet R., Vidal-Madjar A., Gry C., 1985, *ApJ*, 298, 838
- Gaposchkin S., 1955, *Boletin de los Observatorios Tonantzintla y Tacubaya*, 2, 39
- Gershberg R. E., Katsova M. M., Lovkaya M. N., Terebizh A. V., Shakhovskaya N. I., 1999, *A&AS*, 139, 555
- Girardi L., Bressan A., Bertelli G., Chiosi C., 2000, *A&AS*, 141, 371
- Gliese W., 1982, *A&AS*, 47, 471
- Gondoin P., 2007, *A&A*, 464, 1101
- Gray D. F., 1982, *ApJ*, 262, 682
- Gray D. F., 1984, *ApJ*, 281, 719
- Güver T., Özel F., 2009, *MNRAS*, 400, 2050
- Hatzes A. P., 1995, *AJ*, 109, 350
- Ishihara D., Onaka T., Katata H., et al. 2010, *A&A*, 514, A1
- Kupka F., Piskunov N., Ryabchikova T. A., Stempels H. C., Weiss W. W., 1999, *A&AS*, 138, 119
- Lambert D. L., Ries L. M., 1981, *ApJ*, 248, 228
- Lind K., Asplund M., Barklem P. S., 2009, *A&A*, 503, 541
- Maldonado J., Eiroa C., Villaver E., Montesinos B., Mora A., 2012, *A&A*, 541, A40
- Massarotti A., Latham D. W., Stefanik R. P., Fogel J., 2008, *AJ*, 135, 209
- Mathis J. S., 1990, *ARA&A*, 28, 37
- McDowell J., , 1994, *The Einstein Observatory Soft X-ray Source List*
- Montes D., Fernandez-Figueroa M. J., de Castro E., Sanz-Forcada J., 1997, *A&AS*, 125, 263
- Morel M., Magnenat P., 1978, *A&AS*, 34, 477
- Münch L., Münch G., 1955, *Boletin de los Observatorios Tonantzintla y Tacubaya*, 2, 36
- Oláh K., Moór A., Granzer T., Strassmeier K. G., 2013, *Central European Astrophysical Bulletin*, 37, 235
- Pakhomov Y. V., 2013, *Astronomy Letters*, 39, 54
- Pakhomov Y. V., Antipova L. I., Boyarchuk A. A., 2011, *Astronomy Reports*, 55, 256
- Pakhomov Y. V., Chugai N. N., Iyudin A. F., 2012, *MNRAS*, 424, 3145
- Palmerini S., Cristallo S., Busso M., Abia C., Uttenthaler S., Gialanella L., Maiorca E., 2011, *ApJ*, 741, 26
- Petit M., 1958, *Memorie della Societa Astronomica Italiana Suppl.*, 2, 29
- Pettersen B. R., Hawley S. L., 1989, *A&A*, 217, 187
- Pojmanski G., 1997, *Acta Astron.*, 47, 467
- Prugniel P., Vauglin I., Koleva M., 2011, *A&A*, 531, A165
- Ryabchikova T. A., Pakhomov Y. V., Piskunov N. E., 2011, *Kazan Izdatel Kazanskogo Universiteta*, 153, 61
- Saar S. H., 1998, *Information Bulletin on Variable Stars*, 4580, 1
- Saar S. H., Huovelin J., Osten R. A., Shcherbakov A. G., 1997, *A&A*, 326, 741
- Samus N. N., Durlevich O. V., et al., 2009, *General Catalogue of Variable Stars*
- Schröder K.-P., Cuntz M., 2005, *ApJ*, 630, L73
- Schroeder K.-P., Huensch M., Schmitt J. H. M. M., 1998, *A&A*, 335, 591
- Stobie R. S., Ishida K., Peacock J. A., 1989, *MNRAS*, 238, 709
- Tokovinin A. A., 1987, *Soviet Ast.*, 31, 98
- Tsymbal V., Lyashko D., Weiss W. W., 2003, in Piskunov N., Weiss W. W., Gray D. F., eds, *Modelling of Stellar Atmospheres Vol. 210 of IAU Symposium, Processing Stellar Echelle Spectra*. p. 49
- Ulmschneider P., 1979, *Space Sci. Rev.*, 24, 71
- van Leeuwen F., 2007, *A&A*, 474, 653
- Wamsteker W., Skillen I., Ponz J. D., de la Fuente A., Barylak M., Yurrita I., 2000, *Ap&SS*, 273, 155
- Welsh B. Y., Crifo F., Lallement R., 1998, *A&A*, 333, 101
- Welsh B. Y., Lallement R., Vergely J.-L., Raimond S., 2010, *A&A*, 510, A54
- Wright E. L., Eisenhardt P. R. M., Mainzer A. K., et al. 2010, *AJ*, 140, 1868